

Modeling the Dense Spray Regime Using an Euler-Lagrange Approach With Volumetric Displacement Effects

Pedram Pakseresht^a, Sourabh V. Apte^{a,*}

^a*School of Mechanical, Industrial and Manufacturing Engineering, Oregon State University, Corvallis, OR 97331, USA*

Abstract

Modeling of a dense spray regime using an Euler-Lagrange approach is challenging because of local high volume loading. A cluster of droplets, that are assumed subgrid, can lead to locally low void fractions for the fluid phase. Under these conditions, spatio-temporal changes in the fluid volume fractions should be considered in an Euler-Lagrange, two-way coupling model. This leads to zero-Mach number, variable density governing equations. Using pressure-based solvers, this gives rise to a source term in the pressure Poisson equation and a non-divergence free velocity field. To test the validity and predictive capability of such an approach, a round jet laden with particles is investigated using Direct Numerical Simulation coupled with point-Particle based model and compared with available experimental data for a particulate turbulent round jet with $Re_j = 5712$. Standard force closures including drag, lift, Magnus effect, pressure, added mass as well as viscous torque acting on each individual particle are employed in the Point-Particle based model. In addition, volume displacement effects due to the presence of solid particles or liquid droplets, which is commonly neglected in the standard two-way coupling, are taken into account in both continuity and inter-phase momentum transfer to accurately capture the underlying structure of particle-turbulence interactions. Prediction results are in well agreement with the corresponding experiment.

1. Introduction

The performance of aircraft engines depends to a large extent on the efficiency and stability of the combustion process which in turn is extremely sensitive to the spatio-temporal distribution of the fuel/air mixture in the combustor. Fuel injection followed by atomization or breakup in the liquid fuel helps improve the combustion process with increasing the fuel surface area in order to decrease the time required for evaporating the fuel. The numerical models for spray calculations should be able to accurately represent droplet deformation, breakup, collision/coalescence, and dispersion due to turbulence. Significant progress has been made in modeling combustion in engines, yet accurate predictive models and simulation

*Corresponding author. 204 Rogers Hall, Corvallis, OR 97331, USA. Tel: +1 541 737 7335, Fax: +1 541 737 2600. Email address: Sourabh.Apte@oregonstate.edu; pakserrep@oregonstate.edu

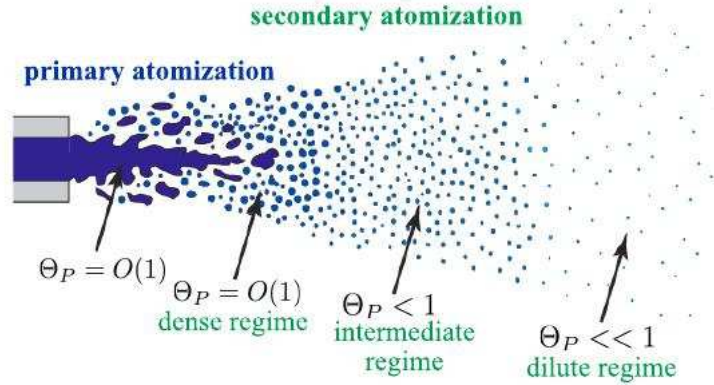


Figure 1: Regimes of liquid spray evolution from injectors in gas-turbine engines

tools for dense spray modeling are still lacking. A standard modeling approach for liquid fuel atomization is to split the process into two subsequent steps: primary followed by secondary atomization shown in Fig. 1. In this work, an Euler-lagrange approach taking into account the effect of finite size dispersed droplets are performed numerically to develop a technique for modeling the dense regime of sprays in the secondary atomization region.

Concerning the combustion process and its efficiency, it is the secondary atomization region where most phase change occurs, since there the liquid/gas surface area is orders of magnitude larger than in the primary atomization region, the gaseous temperature tends to be higher due to the closer proximity to the combustion zone, and the residence time of the liquid in the relatively large secondary atomization region is markedly longer than in the compact primary atomization region. The secondary atomization region is characterized by a vast number of droplets that interact with the surrounding gas transferring mass, momentum, and energy and can be characterized by three different regimes as shown in Fig. 1. In the dense regime close to the primary atomization region, the liquid volume fraction θ_p is in the order of one with liquid droplets undergoing secondary breakup. In the intermediate regime, droplets continue to undergo further disintegration; however, θ_p is now smaller than unity. Finally, in the dilute regime, atomization is rare, θ_p is small, the droplets evaporate, and the fuel vapor mixes with the surrounding hot gases. The characterization of sprays based on physical processes in the different regimes also indicates different methodologies/models necessary to capture the dynamics of different regimes. For example, in the dense and intermediate regimes, not only are droplet deformation, collision, and coalescence important, but noticeable droplet-loading and variations in θ_p are crucial and should be taken into account to capture the spray evolution precisely.

In the traditional approaches for spray modeling, the dynamics of the liquid/air interface are not resolved. In fact, the liquid phase is modeled through either an Eulerian (TFM) approach in which droplet considered to be as a continuous liquid phase or Lagrangian Point-Particle/Parcel method (PP) where droplets are assumed subgrid and their motion is captured by laws for drag, buoyancy and pressure forces, etc. from the gas phase. The effect of the droplets on the gas phase is modeled through two-way coupling of mass, momentum,

and energy exchange Dukowicz (1980). Unlike most of the traditional models in which the liquid phase is assumed to break into a body of droplets as soon as it enters the combustion chamber, i.e. no primary atomization (well-known as Blob hypothesis), the Eulerian-Lagrangian Spray Atomization (ELSA) approach couples the Eulerian mixing description for primary atomization (LES/DNS) with Lagrangian formulation (PP method) for secondary breakup Blokkeel et al. (2003); Lebas et al. (2005). These models were originally derived in the context of RANS turbulence models and assume infinite Weber number; however, extensions to LES formulations have been recently proposed by Chesnel et al. (2011b,a).

Recently, hybrid approaches of DNS method for the primary atomization region and LES (or DNS) coupled with Lagrangian Point-Particle/Parcel approach for solving the gas and liquid phases respectively in the secondary atomization region have been developed by Herrmann (2010b,a, 2011). These hybrid approaches have shown quite success in predicting atomization even in complex aircraft engine injectors (Kim et al. (2014); Li and Soteriou (2013)), yet they currently have major shortcomings. Concerning the secondary atomization particularly, the effect of gas volume displacement due to the attention of droplets in the dense and intermediate regions is neglected and still lacking in the current standard two-way coupling Point-Particle approaches. Thus, to enhance and improve the current Lagrangian PP formulations as accurate predictive tools, accounting for local variations in θ_p is intended in this work. Therefore, the point-particle approach is modified by accounting for the volumetric displacements of the carried phase due to the motion of particles or droplets. The disperse phase also affects the carrier phase through mass, momentum, and energy coupling. The combined effect is termed as ‘volumetric coupling’ which is based on the the original formulation by Dukowicz (1980) and later modified by Joseph et al. (1990). The approach is derived based on mixture theory that accounts for the droplet (or particle) volume fraction in a given computational cell. This effect is important in dense spray regimes, however, are typically ignored in the context of LES or DNS simulations.

Recently, Apte et al. (2008) have shown the effect of volumetric displacements on the carrier fluid in dense particle-laden flows. They compared the results for the carrier phase and the particle dispersion obtained from the point-particle assumption and accounting for volumetric displacement effects to show large differences. If the volume displaced by the disperse phase is taken into account, the velocity field is no longer divergence free in the regions of variations in volume fractions. This has a direct effect on the pressure Poisson equation, altering the pressure field through a local source term. These effects may become important in dense regions of spray system. It was shown in the numerical work of Cihonski et al. (2013) that taking into account the volumetric displacement of fluid even under dilute loading (e.g. a small number of bubbles entrained in a vortex ring) can significantly alter the vortex core for certain combinations of the vortex strengths and bubble sizes. However, computing dense spray systems by accounting for volume displacements due to droplet motion could be numerically challenging. The temporal and spatial variations in fluid volume fractions could be locally large and make the computation numerically unstable. This is specifically true if the inter-phase coupling of mass, momentum, and energy is treated explicitly. In the present work, we focus on non-reacting flows and only momentum exchange between the two-phases is considered. As a step to spray modeling, a particle-

laden turbulent jet flow similar to the secondary atomization region will be carried out using Direct Numerical Simulation (DNS) coupled with Point-Particle/Parcel approach (PP) with quantification of the volumetric displacement effect of droplets on the flow.

2. Methodology

An Eulerian–Lagrangian approach to simulate the finite-size particle–laden turbulent flows is performed in this work. Eulerian framework is used to solve the fluid equations while particles are modeled based on the Point–Particle approach using Lagrangian framework. Equations of both carrier and dispersed phases are expressed below.

2.1. Dispersed phase modeling

In the Point-Particle method (e.g. Maxey (1987); Elghobashi (1991); Squires and Eaton (1991)), motion of small particles in turbulent flow field is described by a complicated integro–differential equation of Maxey and Riley (1983). Unlike body-fitted approaches (e.g. Pakseresht et al. (2012)), the no-slip condition on the surface of particles is not imposed in this approach. The positions and velocities of individual particles are obtained by solving (1).

$$\begin{aligned}\frac{d}{dt}(\mathbf{x}_p) &= \mathbf{u}_p \\ \frac{d}{dt}(\mathbf{u}_p) &= \frac{1}{m_p} \Sigma(\mathbf{F}_p) \\ \frac{d}{dt}(\mathbf{\Omega}_p) &= \frac{1}{i_p} \Sigma(\mathbf{T}_p)\end{aligned}\tag{1}$$

Where m_p , i_p , \mathbf{x}_p , \mathbf{u}_p and $\mathbf{\Omega}_p$ are the mass, moment of inertia, position, translational velocity and rotational velocity of each individual particle respectively. On the other hand, \mathbf{F}_p and \mathbf{T}_p represent deterministic forces and torques respectively acting on each particle including, closure drag by Tennen et al. (2011), shear induced lift force by Saffman (1965), Magnus effect of Rubinow and Keller (1961), added mass, pressure gradient and buoyancy. The effect of history force is neglected in this work as it was observed by Bagchi and Balachandar (2003) to be insignificant. In addition to the forces, rotation and torques of each particle are performed through the closure of hydrodynamic torque given in (3).

$$\mathbf{F}_p = \mathbf{F}_g + \mathbf{F}_{pr} + \mathbf{F}_d + \mathbf{F}_{l,Saff} + \mathbf{F}_{l,Mag} + \mathbf{F}_{am}\tag{2}$$

$$\mathbf{T}_p = \mathbf{T}_h\tag{3}$$

2.2. Hydrodynamic forces and torques

Hydrodynamic forces acting on each individual particle employ closures developed by theory, experiment or fully resolved simulations. Here, closure of all hydrodynamic forces and torques (T_h) as well as gravity and pressure forces are given through (4)-(10).

$$\mathbf{F}_g = -m_p \mathbf{g} \quad (4)$$

$$\mathbf{F}_{pr} = -V_p \nabla P|_p \quad (5)$$

$$\mathbf{F}_d = m_p \frac{C_d(Re_p, \Theta_p)}{\tau_p} (\mathbf{u}_{f|p} - \mathbf{u}_p) \quad (6)$$

$$\begin{aligned} \mathbf{F}_{l,Saff} &= m_p C_l \frac{\rho_f}{\rho_p} (\mathbf{u}_{f|p} - \mathbf{u}_p) \times (\nabla \times \mathbf{u}_f)|_p, \\ C_l &= \frac{1.61 \times 6}{\pi d_p} \sqrt{\frac{\mu_f}{\rho_f} |(\nabla \times \mathbf{u}_f)|_p} \end{aligned} \quad (7)$$

$$\mathbf{F}_{am} = m_p C_{am} \frac{\rho_f}{\rho_p} \left(\frac{D\mathbf{u}_{f|p}}{Dt} - \frac{d\mathbf{u}_p}{dt} \right), \quad C_{am} = 0.5 \quad (8)$$

$$\mathbf{F}_{l,Mag} = C_{mag} \frac{\mathbf{u}_{rel} \times \boldsymbol{\Omega}_{rel}}{|\boldsymbol{\Omega}_{rel}|} \left(\frac{1}{2} \rho_f |\mathbf{u}_{rel}| A \right), \quad \text{and} \quad C_{mag} = \min(0.5, 0.25 \frac{d_p |\boldsymbol{\omega}_{rel}|}{|\mathbf{u}_{rel}|}) \quad (9)$$

$$\mathbf{T}_h = i_p \frac{60}{64\pi} \frac{\rho_f}{\rho_p} C_t |\boldsymbol{\Omega}_{rel}| \boldsymbol{\Omega}_{rel}. \quad (10)$$

where volume and volume fraction of each particle are represented by V_p and Θ_p respectively. $\mathbf{u}_{rel} = \mathbf{u}_{f|p} - \mathbf{u}_p$ is the relative velocity between fluid velocity seen by particle ($\mathbf{u}_{f|p}$) and particle velocity (\mathbf{u}_p) so is the relative rotational velocity ($\boldsymbol{\Omega}_{rel}$). On the other hand, $\tau_p = (\rho_p d_p^2)/(18\rho_f \mu_f \Theta_f)$ and $Re_p = (\Theta_{f|p} \rho_f |\mathbf{u}_{rel}| d_p)/(\mu_f)$ are the respective particle relaxation time and Reynolds number modified with the volumetric displacement effect Finn et al. (2016). C_t in 10 is determined based on work of Pan et al. (2001). Due to high loading of droplets in the dense sprays, modified coefficient of drag based on work of Tennesi et al. (2011) given in 11 is employed here.

$$\begin{aligned} C_d(Re_p, \Theta_p) &= (1 - \Theta_p) \left(\frac{C_d(Re_p, 0)}{(1 - \Theta_p)^3} + A + B \right), \\ A &= \frac{5.81 \Theta_p}{(1 - \Theta_p)^3} + 0.48 \frac{\Theta_p^{1/3}}{(1 - \Theta_p)^4}, \\ B &= \Theta_p^3 Re_p \left(0.95 + \frac{0.61 \Theta_p^3}{(1 - \Theta_p)^2} \right), \\ C_d(Re_p, 0) &= 1 + 0.15 Re_p^{0.687}. \end{aligned} \quad (11)$$

2.3. Fluid Phase Modeling

Direct Numerical Simulation (DNS) is used to solve the fluid equations in structured Cartesian grid using finite volume discretization. A pressure based second order fractional time step method based on work of Cihonski et al. (2013), Finn et al. (2011) and Shams et al. (2011) adjusted to co-located structured grid by Finn et al. (2016) is used here. To consider the effect of fluid volume displaced by the motion of particles, the volume filtered Navier-Stokes equations given in (12)-(13) are applied here Anderson and Jackson (1967).

$$\frac{\partial(\rho_f\theta_f)}{\partial t} + \nabla \cdot (\rho_f\theta_f\mathbf{u}_f) = 0. \quad (12)$$

where ρ_f , θ_f , and \mathbf{u}_f are density, concentration, and velocity of the fluid phase respectively. Fluid concentration is calculated as $\theta_f = 1 - \theta_p$, where θ_p is particle concentration. Local spatio-temporal variations of particle concentration, generate a non-divergence free velocity field in the flow (Pakseresht and Apte, 2017). Modified momentum equations are also given in (13).

$$\begin{aligned} \frac{\partial(\rho_f\theta_f\mathbf{u}_f)}{\partial t} + \nabla \cdot (\rho_f\theta_f\mathbf{u}_f\mathbf{u}_f) = \\ - \nabla P + \nabla \cdot (\mu_f(\nabla\mathbf{u}_f + \nabla\mathbf{u}_f^T - \frac{2}{3}\nabla \cdot \mathbf{u}_f)) \\ - \theta_f\rho_f\mathbf{g} + \mathbf{F}_{p \rightarrow f} + \nabla \cdot \mathbf{T}_{p \rightarrow f}. \end{aligned} \quad (13)$$

In the above form, the conservation equations (i.e. both continuity and momentum equations) account for the volume of fluid displaced by the motion of particles through the fluid volume fraction of θ_f . In addition, (13) also contains the typical inter-phase momentum transfer term (two-way coupling), $\mathbf{F}_{p \rightarrow f}$, based on particle forces. Moreover, to accurately capturing the effect of particles onto the flow, additional inter-phase momentum transfer through the rotation of particles, $\nabla \cdot \mathbf{T}_{p \rightarrow f}$ based on work of Andersson et al. (2012) is added to the momentum equations (referred to as Torque coupling). These terms, $\mathbf{F}_{p \rightarrow f}$ and $\nabla \cdot \mathbf{T}_{p \rightarrow f}$, include the equal and opposite reaction from the particle surface forces and torques respectively back to the flow. Accordingly, it is crucial to define a function, $f(\mathbf{x}, \mathbf{x}_p)$ given in (14) to project Lagrangian quantities of particles, ψ_p , back to the continuous field, ψ_f , located at Eulerian grid points. Likewise, fluid properties are required to be interpolated to the particles' position as well. Gaussian function for both interpolation and projection purposes is employed with bandwidth of local grid size around each particle. It is worth mentioning that giving $\theta_f = 1$ switches the above formulation to the standard two-way coupling where effect of the volume displacement of the carrier phase is neglected.

$$\psi_f(\mathbf{x}) = \sum_{ip=1}^{n_p} f(\mathbf{x}, \mathbf{x}_p)\psi_p \quad (14)$$

3. Results and Discussion

The above numerical scheme is applied to different test cases in order to evaluate its accuracy and robustness (e.g. Pakseresht et al. (2014, 2015, 2016, 2017)). One of these test cases are described below and will be followed by particle-laden turbulent jet as a step in spray modeling.

3.1. Oscillating bubble

First the importance of volumetric displacement effect on the flow field caused by change in local concentration of particles is verified in this section. The variable density formulation used here accounts for changes in the density of mixture. Here, a very simple case of imposed oscillation on the radius of a bubble which causes a potential flow field around itself is set up. This phenomenon can not be simulated by only inter-phase momentum coupling and here it is observed that only through the variations in density in momentum and continuity equation, the potential flow is expressed.

A single air bubble in a cube of water is located and sinusoidal perturbation on the bubble radius is imposed. Bubble radius changes in time as $R = R_0 + e \sin(\omega t)$, where R and R_0 are the instantaneous and the initial radius, respectively, e is the perturbation magnitude, ω is frequency and t is time. In this simulation, $R_0 = 0.01 \times D$, where D is the cube size, and gives overall concentration of 4×10^{-6} , $e = 0.1 \times R_0$, $\omega = 50[Hz]$. Figure 2 shows the radial distribution of hydrodynamic pressure around the bubble created by the size variation at $t^* = 0.3$ where $t^* = t/T$ and $T = 2\pi/\omega$. Analytical solution for pressure (dots), given by Panton (2006) is compared and shown in Fig.2 with result of two-way coupling and no volumetric effect (dashed line). No any effect in the result of two-way coupling for pressure is achieved, however the volumetric coupling result (solid line) is in good agreement with the analytical solution (Shams et al., 2011).

In another similar example, two bubbles oscillating in tandem are considered. Two similar bubbles are put in a box and their radius changes sinusoidally with π [rad] phase shift. All properties are similar to the case of single bubble case, except they are both located $D/6$ away from the box center. The result is a doublet-like flow which is shown in Fig. 3. Likewise, in this case no any effect on the flow is observed by two-way coupling results (Shams et al., 2011).

3.2. Particle-laden turbulent flow

As a step in developing spray modeling, particle-laden turbulent jets have been studied recently (e.g. Shuen et al. (1983)) to obtain the underlying structures of suspended particles and turbulence which could eventually help understand the physics of liquid breakup in the secondary atomization process. Accordingly, in this part, a particle-laden turbulent jet flow performed by Mostafa et al. (1989) is carried out numerically using DNS along with volumetric coupling of Point-Particle tracking approach as a first step in modeling dense sprays. Flow parameters are tabulated in Tab. 1. A Cartesian structured grid is applied for solving the flow in a rectangular computational domain. It is well recognized that properly chosen boundary conditions is of importance in view of a good representation of a physical

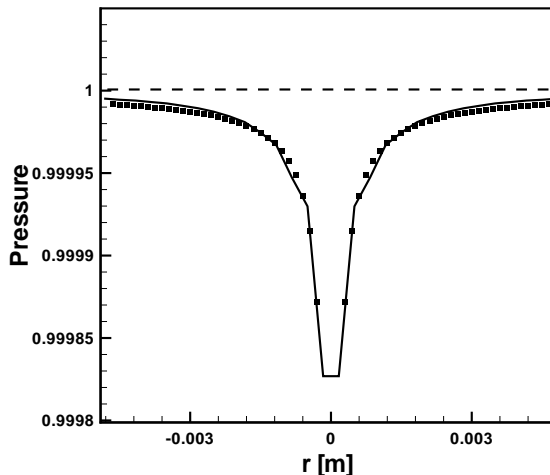


Figure 2: Pressure distribution caused by volume displacement around the bubble, from two-way coupling (dashed line), volumetric coupling (solid line), and analytical solution (dots).

Property	Value	Unit
d_{jet}	0.0253	m
μ_f	1.8502×10^{-5}	$(N.s)m^{-2}$
ρ_f	1.178	kg/m^3
U_{jet}	3.546	ms^{-1}
Re_{jet}	5712	–
d_p	105×10^{-6}	m
ρ_p	2500	kg/m^3
α	1	–

Table 1: Particle-laden jet parameters

jet. Inflow data over several flow through times is generated a priori and read at each flow time step to specify the fluid velocity components at the inlet. Convective outflow boundary condition is applied at the exit section while slip boundary condition is enforced for other sides of the computational domain as shown in Fig. 4. To overcome on the reflection of boundary error from downstream side to the upstream side of the jet due to the hyperbolic characteristic of the convective outlet boundary condition Dai et al. (1994), a long enough computational domain ($30d_j \times 10d_j \times 10d_j$) is used to obtain more accurate results yet more expensive in terms of computational cost.

As mentioned earlier, inflow data is only used for the fluid phase of the flow; however, for solid phase a measured data from experiment is prescribed at the nozzle exit. It is worth mentioning that since no measured data is available right at the nozzle exit, rather at $x/d_{jet} = 0.04$, particles are injected at the nozzle exit based on the provided measured mean

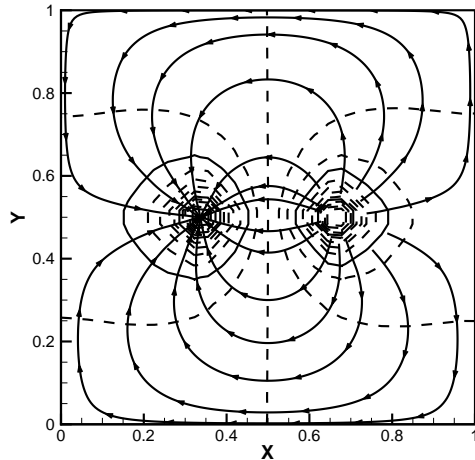


Figure 3: Doublet generated by bubbles oscillating in tandem

and rms fluctuating velocities at $x/d_{jet} = 0.04$ (1 mm from the nozzle exit). Concerning the number of particles, they are injected randomly through the cross section of the jet inlet based on the initial solid-air mass flux rate given in Tab. 1. Total number of particles (n_p) required for injecting per flow time step (Δt_f) is calculated through Eq. 15. It should be emphasized that injection is performed once the particle-free jet (clear jet) has reached to the statistically stable condition. To interpolate gas properties at the position of the solid phase, Gaussian function is employed with filter size of equal to the local grid resolution ($\sigma \sim \Delta$). Similarly, this function with equal filter size is used for projecting the particles' forces back onto the Eulerian framework of the gas phase.

$$n_p = \frac{6\alpha\rho_f d_j^2 u_j \Delta t_f}{4\rho_p d_p^3} \quad (15)$$

Simulations have been performed in the developing ($x/d_j < 6$) and self-similar regions of the two-phase jet close to the nozzle. The results are plotted in a dimensionless form versus normalized radius (r/r_j) to show the spreading of the jet in the radial direction. All quantities except mean axial velocity of the fluid phase are normalized by the local mean centerline velocity (U_c) while mean axial gas velocity is normalized by the initial jet centerline velocity at the nozzle exit (U_0). In this way, the jet centerline velocity decay can be illustrated as well. Figure 5 shows the radial profile of normalized mean axial velocity of the gas phase at the several nozzle distances. As depicted in this figure, mean velocity of the gas phase at different distances from the jet exit is well predicted compared to the experiment. In addition, the decaying and spreading features of the jet can be easily observed in this plot. By getting farther from the nozzle exit, mean velocity of the jet is decayed while the jet is spread more in radial direction.

Likewise, radial profile of the normalized mean axial velocity of the solid phase depicted

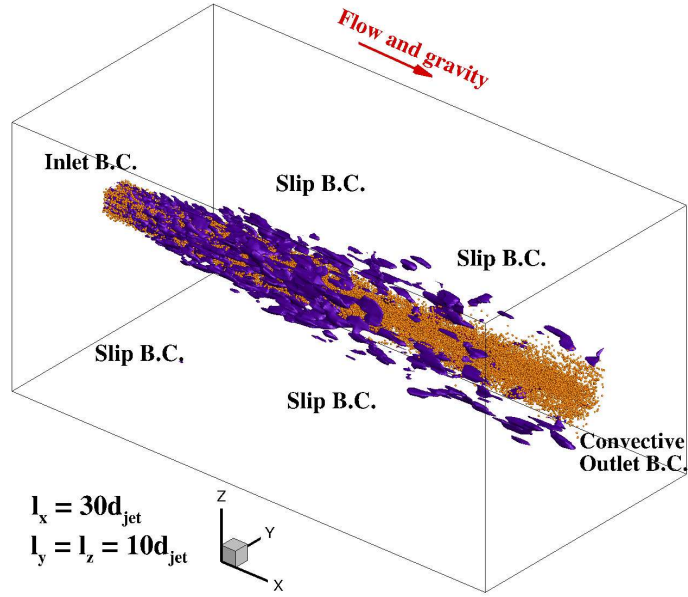


Figure 4: Schematic of particle laden jet with specifying boundary conditions. Vorticity magnitude and particle distribution with exaggerating in particle size for sake of clarity are shown.

in Fig. 6 illustrates a good agreement between simulation and the experiment; however, slightly under prediction in the edge of the jet is noticeable in the simulation. It should be emphasized that similar results for the solid phase were obtained in the numerical prediction part of Mostafa et al. (1989) (not shown here). This discrepancy between numerical simulation and experiment for solid phase can be addressed as a result of inappropriate inflow data for solid phase. Particles would have been more accurately predicted if they had been generated *a priori* in line with gas phase. As a result, a remedy to overcome this discrepancy would be generating the inflow data in which particles have been already injected and interacted with the carrier phase. This would definitely affect the carrier phase and give rise to accurately improve the simulation results.

Further insight can be obtained by looking at the dynamics of the particle laden-jet flow through the calculation of rms of fluctuating axial velocity for fluid phase. As shown in Fig. 7, for the region of $x/d_j > 2.08$, it can be clearly seen that simulation for rms of gas phase is within the range of experiment with slightly lower values in $r/r_j > 0.5$ as well as significant under prediction in the radial region of $r/r_j < 0.5$ compared to the experiment. This reveals the fact that the grid resolution is not sufficient to capture all the smallest scales embedded in the gas phase. Higher resolution would definitely help improve the rms of fluid particularly in the shear region of the jet where high gradient of velocity exists.

Finally, the axial profile of the predicted mean velocity in the center of the jet for both phases compared to the experiment are plotted in Fig.8. The velocity profile for each phase is normalized by its corresponding mean velocity in the center of the nozzle exit (i.e. U_{f0} for gas phase and U_{p0} for solid phase). As depicted in this figure, both phases are well predicted in the center line mean velocity; however, slightly higher velocity for solid phase while lower

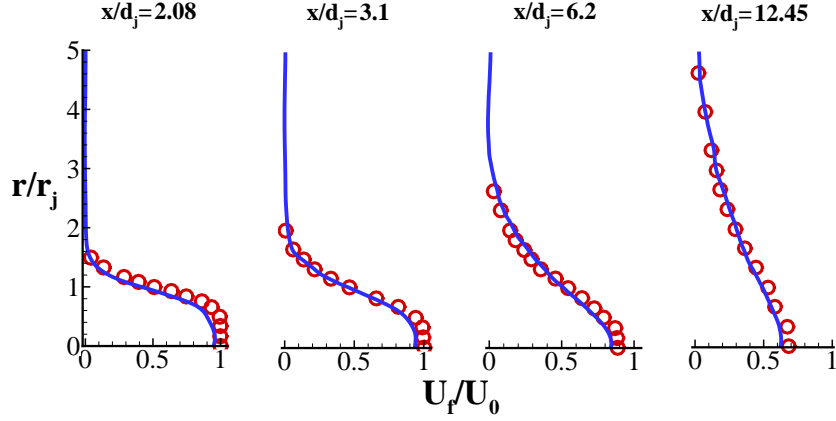


Figure 5: Radial profile of normalized mean axial velocity of the gas phase, solid line: simulation, open symbol: experiment

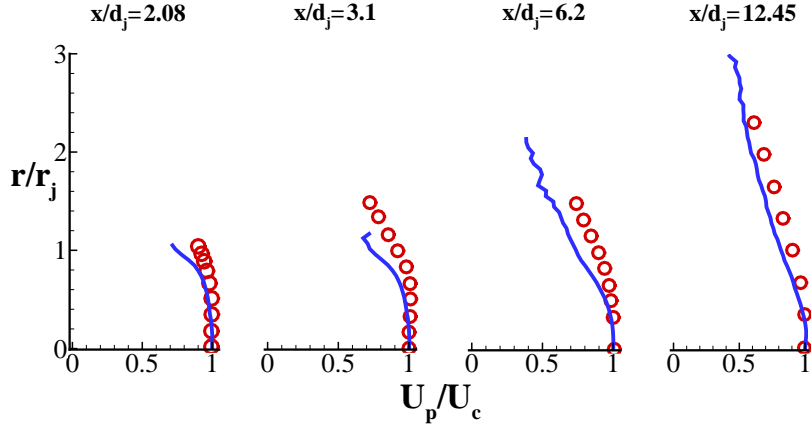


Figure 6: Radial profile of normalized mean axial velocity of the solid phase, solid line: simulation, open symbol: experiment

velocity for gas phase is noticeable in the simulation.

4. Summary and conclusion

A numerical formulation based on co-located grid, finite volume approach is developed for simulation of dense particle-laden flows. Direct Numerical Simulation coupled with point-particle method was performed to model the interactions of particle and turbulence in the particle-laden jet flows as well as secondary atomization region in sprays. Volumetric displacement effect of fluid due to presence of liquid particles was taken into account to capture accurately the underlying structure of particle-laden turbulent flows. Several test cases were considered to evaluate the accuracy and robustness of the numerical scheme for dense loadings. First, the effect of a single bubble undergoing forced periodic oscillations was computed by considering the present approach as well as the standard ‘two-way’ coupling

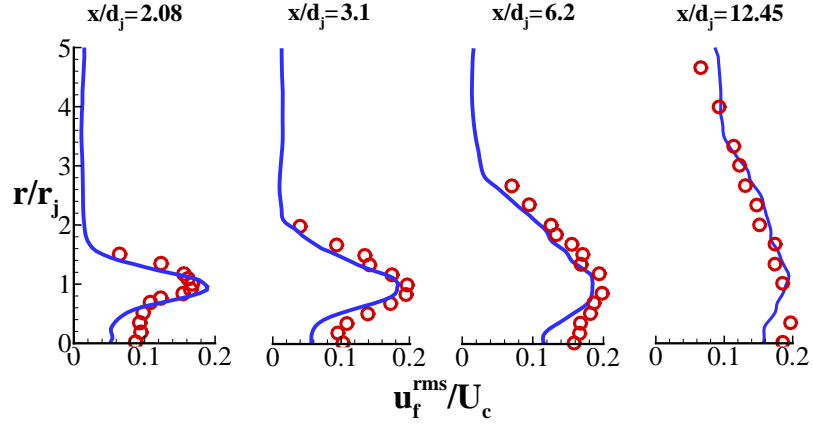


Figure 7: Radial profile of normalized axial fluctuating velocity of gas phase, solid line: simulation, open symbol: experiment

based point-particle method to show large variations in the predicted flow field. The results were compared with analytical solutions to validate the numerical approach for volumetric coupling. A test case with two bubbles undergoing forced oscillations in tandem was also investigated. The doublet-like flow pattern was well predicted by the present approach. Next, a particle-laden turbulent round jet with $Re = 5712$ based on work of Mostafa et al. (1989) was simulated to test the robustness of the numerical scheme with taking into account the volumetric displacement of fluid due to presence of particles. The present numerical approach is capable to simulate the dense regime of particle-laden turbulent jet flows or sprays.

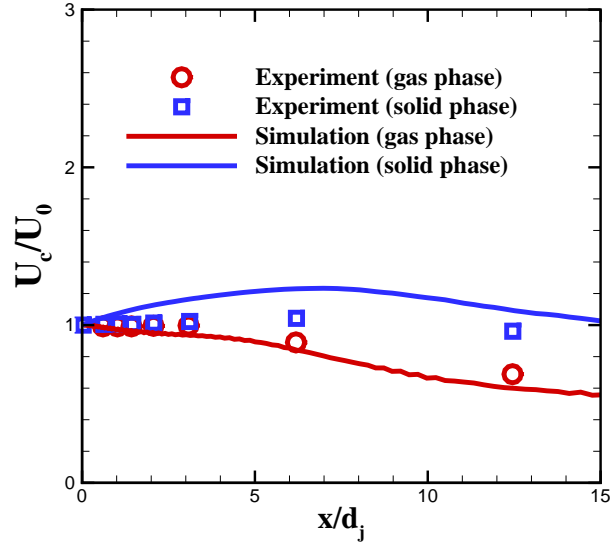


Figure 8: Centerline velocity for both gas and solid phases

5. Nomenclature

d_{jet}	Jet diameter
d_p	Particle diameter
Re_{jet}	Jet Reynolds number
U_{jet}	Jet bulk velocity
ρ_p	Particle density
α	Mass loading
μ_f	Air viscosity
ρ_f	Air density
St	Stokes number
τ_p	Particle relaxation time
m_p	Particle mass
i_p	Particle inertia
\mathbf{u}_p	Particle translational velocity vector
$\mathbf{\Omega}_p$	particle rotational velocity vector
\mathbf{F}_p	Deterministic particle force
\mathbf{T}_p	Deterministic particle torque
V_p	Particle volume
θ_p	Volume fraction of particle
\mathbf{u}_{rel}	Relative velocity between phases
$\mathbf{u}_{f p}$	Fluid velocity seen by particle

References

- Anderson, T. B., Jackson, R., 1967. Fluid mechanical description of fluidized beds. equations of motion. *Industrial & Engineering Chemistry Fundamentals* 6 (4), 527–539.
- Andersson, H. I., Zhao, L., Barri, M., 2012. Torque-coupling and particle–turbulence interactions. *Journal of Fluid Mechanics* 696, 319–329.
- Apte, S., Mahesh, K., Lundgren, T., 2008. Accounting for finite-size effects in simulations of disperse particle-laden flows. *International Journal of Multiphase Flow* 34 (3), 260–271.
- Bagchi, P., Balachandar, S., 2003. Effect of turbulence on the drag and lift of a particle. *Physics of fluids* 15 (11), 3496–3513.
- Blokkeel, G., Barbeau, B., Borghi, R., 2003. A 3d eulerian model to improve the primary breakup of atomizing jet. Tech. rep., SAE Technical Paper.
- Chesnel, J., Menard, T., Reveillon, J., Demoulin, F.-X., 2011a. Subgrid analysis of liquid jet atomization. *Atomization and Sprays* 21 (1).
- Chesnel, J., Reveillon, J., Menard, T., Demoulin, F.-X., 2011b. Large eddy simulation of liquid jet atomization. *Atomization and Sprays* 21 (9).
- Cihonski, A. J., Finn, J. R., Apte, S. V., 2013. Volume displacement effects during bubble entrainment in a travelling vortex ring. *Journal of Fluid Mechanics* 721, 225–267.
- Dai, Y., Kobayashi, T., Taniguchi, N., 1994. Large eddy simulation of plane turbulent jet flow using a new outflow velocity boundary condition. *JSME International Journal Series B Fluids and Thermal Engineering* 37 (2), 242–253.
- Dukowicz, J. K., 1980. A particle–fluid numerical model for liquid sprays. *Journal of Computational Physics* 35 (2), 229–253.
- Elghobashi, S., 1991. Particle-laden turbulent flows: direct simulation and closure models. *Applied Scientific Research* 48 (3-4), 301–314.
- Finn, J., Shams, E., Apte, S. V., 2011. Modeling and simulation of multiple bubble entrainment and interactions with two dimensional vortical flows. *Physics of Fluids* 23 (2), 023301.
- Finn, J. R., Li, M., Apte, S. V., 2016. Particle based modelling and simulation of natural sand dynamics in the wave bottom boundary layer. *Journal of Fluid Mechanics* 796, 340–385.
- Herrmann, M., 2010a. Detailed numerical simulations of the primary atomization of a turbulent liquid jet in crossflow. *Journal of Engineering for Gas Turbines and Power* 132 (6), 061506.
- Herrmann, M., 2010b. A parallel eulerian interface tracking/lagrangian point particle multi-scale coupling procedure. *Journal of Computational Physics* 229 (3), 745–759.
- Herrmann, M., 2011. On simulating primary atomization using the refined level set grid method. *Atomization and Sprays* 21 (4).
- Joseph, D., Lundgren, T., Jackson, R., Saville, D., 1990. Ensemble averaged and mixture theory equations for incompressible fluid–particle suspensions. *International journal of multiphase flow* 16 (1), 35–42.
- Kim, D., Ham, F., Le, H., Herrmann, M., Li, X., Soteriou, M., Kim, W., 2014. High-fidelity simulation of atomization in a gas turbine injector high shear nozzle. In: *ILASS Americas 26th Annual Conference on Liquid Atomization and Spray Systems*, Portland, OR, May. pp. 18–21.
- Lebas, R., Blokkeel, G., Beau, P.-A., Demoulin, F.-X., 2005. Coupling vaporization model with the eulerian-lagrangian spray atomization (elsa) model in diesel engine conditions. Tech. rep., SAE Technical Paper.
- Li, X., Soteriou, M., 2013. High-fidelity simulation of fuel atomization in a realistic swirling flow injector. *Atomization and Sprays* 23 (11).
- Maxey, M., 1987. The gravitational settling of aerosol particles in homogeneous turbulence and random flow fields. *Journal of Fluid Mechanics* 174, 441–465.
- Maxey, M. R., Riley, J. J., 1983. Equation of motion for a small rigid sphere in a nonuniform flow. *The Physics of Fluids* 26 (4), 883–889.
- Mostafa, A., Mongia, H., McDonell, V., Samuelsen, G., 1989. Evolution of particle-laden jet flows—a theoretical and experimental study. *AIAA journal* 27 (2), 167–183.
- Pakseresht, P., Apte, S., Finn, J., 2014. Interactions of turbulence and sediment particles in an open channel flow. In: *APS Meeting Abstracts*.

- Pakseresht, P., Apte, S., Finn, J., 2015. Dns with discrete element modeling of suspended sediment particles in an open channel flow. In: APS Division of Fluid Dynamics Meeting Abstracts.
- Pakseresht, P., Apte, S., Finn, J., 2016. Dns-dem of suspended sediment particles in an open channel flow. In: APS Meeting Abstracts.
- Pakseresht, P., Apte, S. V., 2017. Prediction of a densely loaded particle-laden jet using a euler-lagrange dense spray model. In: APS Division of Fluid Dynamics Meeting Abstracts.
- Pakseresht, P., Apte, S. V., Finn, J. R., 2017. On the predictive capability of dns-dem applied to suspended sediment-turbulence interactions. In: ASME 2017 Fluids Engineering Division Summer Meeting. American Society of Mechanical Engineers Digital Collection.
- Pakseresht, P., Bahrainian, S., Bahoosh Kazerooni, R., 2012. An algorithm in element deletion process used in moving three zones unstructured grid for arbitrary relative motion of two objects. In: Proceedings of 3 rd International Conference on Theoretical and Applied Mechanics, Athens, Gr.
- Pan, Y., Tanaka, T., Tsuji, Y., 2001. Direct numerical simulation of particle-laden rotating turbulent channel flow. *Physics of Fluids* 13 (8), 2320–2337.
- Panton, R., 2006. *Incompressible Flow*. Wiley-Interscience.
- Rubinow, S., Keller, J. B., 1961. The transverse force on a spinning sphere moving in a viscous fluid. *Journal of Fluid Mechanics* 11 (03), 447–459.
- Saffman, P., 1965. The lift on a small sphere in a slow shear flow. *Journal of fluid mechanics* 22 (02), 385–400.
- Shams, E., Finn, J., Apte, S., 2011. A numerical scheme for euler–lagrange simulation of bubbly flows in complex systems. *International Journal for Numerical Methods in Fluids* 67 (12), 1865–1898.
- Shuen, J., Chen, L., Faeth, G., 1983. Predictions of the structure of turbulent, particle-laden round jets. *AIAA journal* 21 (11), 1483–1484.
- Squires, K. D., Eaton, J. K., 1991. Preferential concentration of particles by turbulence. *Physics of Fluids A: Fluid Dynamics* 3 (5), 1169–1178.
- Tenneti, S., Garg, R., Subramaniam, S., 2011. Drag law for monodisperse gas–solid systems using particle-resolved direct numerical simulation of flow past fixed assemblies of spheres. *International journal of multiphase flow* 37 (9), 1072–1092.